

RESEARCH ARTICLE

An efficient quasi-Newton method for 2D steady free surface flow

Toon Demeester¹ | E. Harald van Brummelen² | Joris Degroote^{1,3}

¹Department of Flow, Heat and Combustion Mechanics, Ghent University, Ghent, Belgium

²Department of Multiscale Engineering Fluid Dynamics, Eindhoven University of Technology, Eindhoven, the Netherlands

³Flanders Make, Belgium

Correspondence

Toon Demeester, Department of Flow, Heat and Combustion Mechanics, Ghent University, Sint-Pietersnieuwstraat 41, 9000 Gent, Belgium. Email: toon.demeester@ugent.be

Summary

Steady free surface flows are of interest in the fields of marine and hydraulic engineering. Fitting methods are generally used to represent the free surface position with a deforming grid. Existing fitting methods tend to use time-stepping schemes, which is inefficient for steady flows. There also exists a steady iterative method, but that one needs to be implemented with a dedicated solver. Therefore a new method is proposed to efficiently simulate 2D steady free surface flows, suitable for use in conjunction with black-box flow solvers. The free surface position is calculated with a quasi-Newton method, where the approximate Jacobian is constructed in a novel way by combining data from past iterations with an analytical model based on a perturbation analysis of a potential flow. The method is tested on two 2D cases: the flow over a bottom topography and the flow over a hydrofoil. For all simulations the new method converges exponentially and in few iterations. Furthermore, convergence is independent of the free surface mesh size for all tests.

KEYWORDS:

Free Surface Flow, Fitting Method, Perturbation Analysis, Quasi-Newton

1 | INTRODUCTION

This paper considers the numerical simulation of steady free surface flow of incompressible, immiscible fluids with a large density difference, typically water and air. This type of flow is often encountered in the fields of marine and hydraulic engineering, for example to calculate ship hull resistance, analyze ship-wall interactions in narrow straight canals and study flow behavior in river confluences. These flows are governed by the incompressible Navier-Stokes equations, which are typically solved with computational fluid dynamics (CFD).

The free surface causes additional difficulties for the flow computations: its position is unknown a priori, and needs to be determined as a component of the solution during the computation. Two classes of methods exist to represent the free surface, viz. surface capturing and surface fitting methods.[†] In surface capturing approaches, the computational mesh is not aligned with the interface, and the interface can intersect the mesh in an in principle arbitrary manner. Capturing methods are versatile in that they can handle complex phenomena such as wave breaking. Examples are the marker-and-cell method², the volume-of-fluid method³ and the level-set method.⁴

The second class of approaches is surface fitting, where the computational mesh is aligned with the interface. Surface fitting methods enable enforcement of the interface conditions via boundary conditions, and are generally more robust and for the same computational costs more accurate than capturing methods. Surface fitting approaches are therefore the method of choice for free surface flows without topological changes such as wave breaking. Due to the large density difference with water, the air phase can be neglected for these flows so that the free surface becomes a domain boundary. The position of the free surface

[†]Classification and terminology of these methods tends to be inconsistent in literature; terminology is adopted from Wackers et al.¹

then depends on kinematic and dynamic boundary conditions, which are derived from the interface conditions. The kinematic boundary condition (KBC) requires that the free surface is impermeable: in steady flows the velocity vectors must be tangent to the free surface. The dynamic boundary condition (DBC) requires continuity of the normal and tangential stresses at the free surface, resulting in respectively the normal DBC and tangential DBC. When the air phase is neglected, shear stresses at the surface are zero, which reduces the DBC to a condition of constant (atmospheric) pressure along the free surface.

The KBC and DBC cannot be imposed simultaneously at the free surface if its position is given. More precisely, the number of boundary conditions at the free surface for this free-boundary problem, is one more than the number of boundary conditions required to solve the incompressible Navier-Stokes equations for a given free surface.⁵ Therefore this problem is solved in an iterative way by distributing the free surface conditions over two steps: a first step in which the flow is solved for a given free surface position and a second step in which a new free surface position is calculated. This iterative process has converged when both KBC and DBC are fulfilled to the required precision.

In the literature several methods can be found which solve this free-boundary problem. They can be distinguished by the way the boundary conditions are distributed over the two steps, and consequently how the new free surface position is calculated in each iteration. Most methods use the DBC in the flow solver and the KBC to calculate the free surface position.^{6,7} This results in a time-stepping scheme due to the time-dependence of the KBC. To reach a steady state solution transient phenomena must decay, which often requires a large number of time-steps owing to weak dissipation. The *steady iterative method* by van Brummelen et al.⁵ avoids this by using the normal DBC for the position calculation. A combined condition (KBC and DBC) is used in the flow solver, thereby improving the coupling between the two steps, which results in good convergence properties of the iterative method. Implementing this method is however not trivial: the combined free surface condition requires a specialized coupled flow solver.

An alternative approach to tackle the free-boundary problem could be to solve the flow equations and the free surface boundary conditions in a monolithic way, to obtain the flow variables and the free surface position simultaneously. Although this might be possible for simple 2D cases, it would become unfeasible for realistic 3D problems and is therefore not considered here.

The aim of this paper is to present a new free surface method which converges in a low number of iterations to a steady solution, and can be used with a general purpose black-box flow solver, thereby avoiding the disadvantages of existing methods. With *black-box* it is meant that the source code of the flow solver is not available, such that the solver can only be executed. This black-box compatibility allows the user to replace the flow solver by another one, so as to benefit from the maturity and versatility of existing solvers. A different distribution of the free surface conditions is necessary to accomplish this. The KBC and tangential DBC are enforced in the black-box flow solver by using a free-slip boundary condition at the free surface. An efficient quasi-Newton method based on the normal DBC is then used to calculate the free surface position. The iterations converge fast thanks to the novel way in which the Jacobian is approximated: a Jacobian generated with data gathered during the iterations is combined with a Jacobian derived from an analytical model (based on potential flow).

Section 2 presents the governing equations and gives a more detailed description of the free surface boundary conditions. In Section 3 the quasi-Newton method to solve the free surface problem is presented, using the results of a potential flow perturbation analysis. Section 4 demonstrates the performance of the new method by calculating the 2D free surface flow for two test cases and comparing the results to literature.

2 | PROBLEM DESCRIPTION

This section briefly describes the governing equations for steady free surface flow. The KBC and DBC are then discussed and reduced to the form which is generally used with fitting approaches.

Some notations are introduced first. Vectors and tensors are denoted with respectively a single and double bar notation, e.g. \bar{u} and $\bar{\sigma}$. The Cartesian base vectors are \bar{e}_x and \bar{e}_y . Normal and tangential unit vectors with respect to a given surface are \bar{e}_n and \bar{e}_t . All matrices are denoted by bold symbols. When the free surface is discretized, the discretized variables are represented by a column vector, e.g. the free surface height $\eta(x)$ will have a discrete counterpart $\boldsymbol{\eta} \in \mathbb{R}^{n \times 1}$ with n the number of free surface nodes. A superscript (usually m) is used to denote the iteration index of the fitting method. Differences between values from consecutive iterations are written in the form $\Delta \boldsymbol{\eta}^m = \boldsymbol{\eta}^{m+1} - \boldsymbol{\eta}^m$.

The two-dimensional, steady state flow of an incompressible, Newtonian fluid is considered in this paper. It is described by the steady continuity and Navier-Stokes equations

$$\nabla \cdot \bar{\mathbf{u}} = 0 \quad (1)$$

$$\rho \nabla \cdot \bar{\mathbf{u}}\bar{\mathbf{u}} = -\nabla p + \rho \bar{\mathbf{g}} + \nabla \cdot \bar{\boldsymbol{\tau}} \quad (2)$$

which are solved for the pressure $p(x, y)$ and the velocity vector $\bar{\mathbf{u}}(x, y)$ with components u_x and u_y . ρ is the constant density and $\bar{\mathbf{g}} = -g\bar{\mathbf{e}}_y$ the gravitational acceleration in the negative y -direction. The viscous stress tensor $\bar{\boldsymbol{\tau}}$ is defined as

$$\bar{\boldsymbol{\tau}} = \mu_{\text{eff}} (\nabla \bar{\mathbf{u}} + (\nabla \bar{\mathbf{u}})^T) \quad \text{with} \quad \mu_{\text{eff}} = \mu + \mu_t \quad (3)$$

where the turbulent viscosity μ_t —obtained solving the Reynolds-averaged Navier-Stokes (RANS) equations—is included in the effective dynamic viscosity coefficient μ_{eff} .

Furthermore, a free surface is considered whose location can be expressed as a height function $\eta(x)$. When the air-phase is neglected because of the large density difference, the interface conditions between water and air become boundary conditions at the free surface. The KBC states that the free surface is impermeable. For steady flow this means that the velocity vector at the free surface must be tangent to the free surface. This is expressed in terms of the velocity components as

$$\frac{\partial \eta}{\partial x} = \frac{u_y}{u_x}. \quad (4)$$

The DBC requires continuity of the stresses at the interface. Neglecting surface tension, this means $\bar{\boldsymbol{\sigma}} \cdot \bar{\mathbf{e}}_n$ must be constant at the interface, with

$$\bar{\boldsymbol{\sigma}} = -p\bar{\mathbf{I}} + \bar{\boldsymbol{\tau}}. \quad (5)$$

On the air side, shear stresses are neglected and pressure is assumed equal to p_{cst} over the whole surface. The tangential and normal DBCs become

$$\bar{\mathbf{e}}_t \cdot \bar{\boldsymbol{\tau}} \cdot \bar{\mathbf{e}}_n = 0, \quad (6)$$

$$\bar{\mathbf{e}}_n \cdot \bar{\boldsymbol{\sigma}} \cdot \bar{\mathbf{e}}_n = -p_{\text{cst}}. \quad (7)$$

The latter can be simplified for the flows under consideration, as is frequently done in literature.^{5,6,7} It is assumed that the viscous contribution to the normal stress component at the free surface is negligible with respect to the pressure contribution. In that case the normal DBC from Eq. (7) can be approximated as

$$p = p_{\text{cst}}. \quad (8)$$

When the free surface is modeled as a free-slip wall when numerically solving the Navier-Stokes equations, both the KBC (Eq. (4)) and tangential DBC (Eq. (6)) are automatically satisfied, while the normal DBC (Eq. (7) or simplified in Eq. (8)) is not.

3 | FREE SURFACE QUASI-NEWTON METHOD WITH LEAST-SQUARES AND SURROGATE

When the water-air interface is represented by surface fitting, the steady free surface problem becomes a free-boundary problem. In this section an efficient quasi-Newton solution technique is developed step by step to solve this free-boundary problem. In Section 3.1 a perturbation analysis of potential flow over a flat bottom is described. This analysis demonstrates the fundamental difference between subcritical and supercritical flows, and provides an approximate relation between pressure and height of the free surface. In Section 3.2 this relation is used to construct a surrogate model of the viscous flow solver that will be used as black-box in the method. The new quasi-Newton solution method is proposed in Section 3.3 for supercritical flows, using this surrogate model in combination with a least-squares technique to form the approximate Jacobian. The method is accordingly called *Free surface Quasi-Newton method with Least-Squares and Surrogate*, abbreviated as *FreQ-LeSS* (phonetically *freckles*). Finally, in Section 3.4 the modifications required to extend the problem formulation to subcritical flows are introduced.

3.1 | Relation between pressure and height perturbations at the free surface for potential flow

While viscous flow as described by the Navier-Stokes equations is considered in this paper, it is simplified to potential flow in this section for the purpose of doing a perturbation analysis and deriving a surrogate model. The steady state solution of a 2D

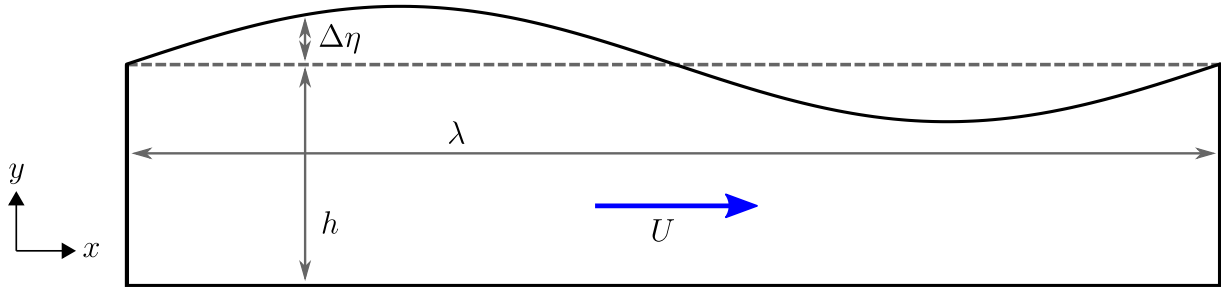


FIGURE 1 Flow over a horizontal plate with sinusoidal perturbation $\Delta\eta$ of the free surface.

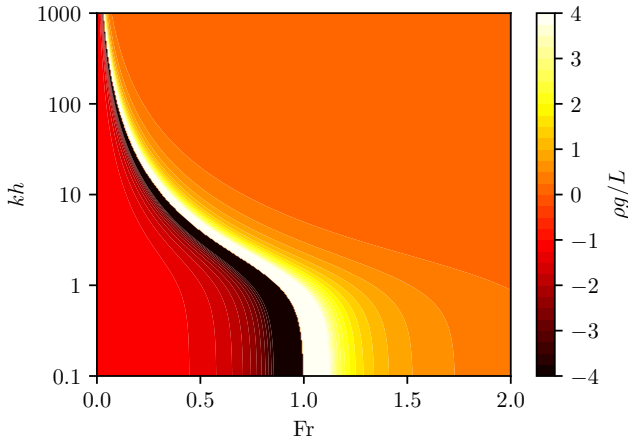


FIGURE 2 $\rho g/L$ as a function of Fr and kh .

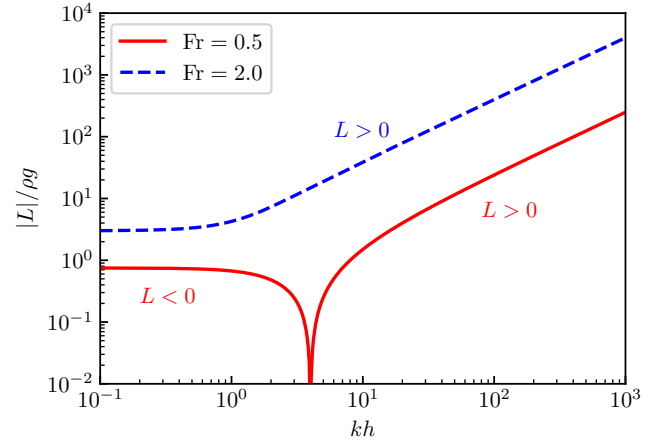


FIGURE 3 $|L|$ as a function of kh for two Fr. Note that for Fr = 0.5 the first part of L is negative (see also Fig. 2).

potential flow over a horizontal plate is a flat free surface: for $\eta(x) = h$ with h an arbitrary depth, the free surface pressure $p(x, \eta(x))$ will be constant (DBC) and the streamlines parallel to the surface (KBC). If the height η of the surface is perturbed with an arbitrary $\Delta\eta$ (see Fig. 1), the pressure will change with a certain Δp . A relation between $\Delta\eta$ and Δp was derived by Demeester et al.⁸ for small perturbations. The conclusions are summarized here.

As shown in Fig. 1, the free surface height is perturbed with

$$\Delta\eta = a \sin(kx + \theta) \quad (9)$$

where $k = 2\pi/\lambda$ is the wavenumber, θ an arbitrary phase angle and the amplitude a small relative to the wavelength λ and depth h . The pressure perturbation Δp then follows from a proportionality relation:

$$\Delta p = L \Delta\eta \quad (10)$$

with

$$L = \rho g \left(\text{Fr}^2 \frac{kh}{\tanh kh} - 1 \right). \quad (11)$$

ρ is the fluid density, g the gravitational acceleration and $\text{Fr} = U/\sqrt{gh}$ the Froude number based on the depth h and the average flow velocity U . The Froude number gives a measure of the relative importance of inertial forces with respect to gravitational forces. Eq. (11) is graphically shown in Fig. 2 as a function of the dimensionless groups kh and Fr. For clarity $\rho g/L$ is plotted instead of L . An asymptote splits the figure in a region where gravitational forces dominate the flow (lower left corner) and a region where inertial forces dominate near the free surface. At the asymptote (where $1/L \rightarrow \pm\infty$ or $L \rightarrow 0$), the opposing effects of gravity and inertia on Δp balance each other. If L is set to zero in Eq. (11), the dispersion relation for gravitational waves is found (neglecting surface tension, see⁹). As a consequence, waves with $L = 0$ have their phase velocity equal to the average flow velocity U , so that they appear stationary. These so-called *steady gravity waves* are solutions of the linearized free surface problem and have $\Delta p = 0$ for a non-zero $\Delta\eta$ of this wavenumber. L can be zero only if the flow is subcritical ($\text{Fr} < 1$), see $1/L$ in Fig. 2 and $|L|$ in Fig. 3. In that case no unique η corresponds to a given p , which complicates finding a unique solution for

the steady free surface problem. For this reason, the new solution method will first be developed for supercritical flows ($Fr > 1$) and then the problem formulation will be expanded to subcritical flows.

3.2 | Surrogate model for viscous flow solver based on potential flow

Consider a numerical simulation where the free surface is discretized in the x -direction with n equidistant points, with the height values collected in an array $\boldsymbol{\eta} \in \mathbb{R}^{n \times 1}$. It is assumed that these points are ordered from inlet to outlet, i.e. $\boldsymbol{\eta}(0)$ and $\boldsymbol{\eta}(n-1)$ are respectively the free surface heights at inlet and outlet of the domain. The pressure values in these points are collected in $\boldsymbol{p} \in \mathbb{R}^{n \times 1}$.

The perturbed flow over a horizontal plate as described in Section 3.1 can also be simulated with a CFD solver $\boldsymbol{F}(\boldsymbol{\eta}) = \boldsymbol{p}$, represented by a (possibly black-box) non-linear function \boldsymbol{F} , returning the free surface pressure \boldsymbol{p} for an arbitrary input height $\boldsymbol{\eta}$. A linear approximation of \boldsymbol{F} is provided by the Jacobian \boldsymbol{F}' :

$$\boldsymbol{F}' \Delta \boldsymbol{\eta} = \Delta \boldsymbol{p} \quad (12)$$

A surrogate model is now constructed for \boldsymbol{F}' , which will be used in Section 3.3 to construct the approximate Jacobian for the new quasi-Newton solution technique. As the fitting method is tested on 2D cases with a uniform free surface mesh in this paper, it is convenient to base the surrogate model on a Fourier series decomposition, although other choices are possible and will be developed for stretched surface meshes in the future.

A height perturbation $\Delta \boldsymbol{\eta}$ (not necessarily small) can now be decomposed into n real Fourier modes: a constant mode, $\text{floor}(n/2)$ cosine modes and $\text{floor}((n-1)/2)$ sine modes. It is assumed that for each[‡] mode Eq. (11) is approximately valid, so that the corresponding $\Delta \boldsymbol{p}$ can be estimated. This operation can be written in matrix form as

$$\Delta \boldsymbol{p} = \boldsymbol{F} \Delta \boldsymbol{\eta} = \sum_{j=0}^{n-1} L_j \boldsymbol{\Phi}_j \Delta \boldsymbol{\eta} \quad (13)$$

with

$$\boldsymbol{\Phi}_j = \boldsymbol{\phi}_j \boldsymbol{\phi}_j^T \quad (14)$$

where $\boldsymbol{\phi}_j \in \mathbb{R}^{n \times 1}$ is the normalized basis vector for Fourier mode j and L_j the corresponding factor from Eq. (11).

If there is a difference between inlet and outlet height, erroneous high frequency components appear in the Fourier decomposition. The solution is to subtract a sawtooth wave such that inlet and outlet heights become equal. The sawtooth (st) that needs to be subtracted to match both ends of the free surface, is identified by multiplying $\Delta \boldsymbol{\eta}$ with the matrix

$$\boldsymbol{\Phi}_{\text{st}} = \begin{bmatrix} \frac{1}{2} & 0 & \dots & 0 & -\frac{1}{2} \\ \vdots & \vdots & & \vdots & \vdots \\ \frac{1}{2} & -\frac{i}{n-1} & 0 & 0 & \frac{i}{n-1} - \frac{1}{2} \\ \vdots & \vdots & \vdots & \vdots & \vdots \\ -\frac{1}{2} & 0 & \dots & 0 & \frac{1}{2} \end{bmatrix} \quad (15)$$

where $\boldsymbol{\Phi}_{\text{st}} \in \mathbb{R}^{n \times n}$ and i is the row index which starts from zero. The sawtooth component is considered to have wavenumber zero (it is multiplied with L_0), instead of being decomposed into a spectrum of low and high frequencies. Eq. (13) is accordingly adapted to

$$\Delta \boldsymbol{p} = \boldsymbol{F}_{\text{st}} \Delta \boldsymbol{\eta} = (\boldsymbol{L}_0 \boldsymbol{\Phi}_{\text{st}} + \boldsymbol{F} (\boldsymbol{I}_n - \boldsymbol{\Phi}_{\text{st}})) \Delta \boldsymbol{\eta}. \quad (16)$$

The matrix $\boldsymbol{F}_{\text{st}}$ serves as a surrogate model for \boldsymbol{F}' . If \boldsymbol{F} is a solver for a more complex 2D free surface flow (viscous flow, different geometry etc.), $\boldsymbol{F}_{\text{st}}$ may still be an adequate approximation to the Jacobian. The surrogate model $\boldsymbol{F}_{\text{st}}$ can only be used when the free surface grid is equidistant in the x -direction. An alternative surrogate model¹⁰ that performs well on non-equidistant grids is not detailed here.

$\boldsymbol{F}_{\text{st}}$ can provide some insight into the behavior of \boldsymbol{F} . For supercritical flow, L is always positive and non-zero, so that $\boldsymbol{F}_{\text{st}}$ is a full rank matrix and thus invertible. This suggests that \boldsymbol{F} is a bijective function, i.e. for every $\boldsymbol{\eta}$ there is a unique \boldsymbol{p} and vice-versa. For subcritical flow, L is zero for one wavenumber and hence $\boldsymbol{F}_{\text{st}}$ is singular.[§] Each wavenumber corresponds to two Fourier-modes (sine and cosine), so the rank of $\boldsymbol{F}_{\text{st}}$ is then $n-2$. To get a unique $\Delta \boldsymbol{\eta}$ for a given $\Delta \boldsymbol{p}$, two extra conditions on $\Delta \boldsymbol{\eta}$ are required. It is assumed that this reasoning also holds for a general \boldsymbol{F} with subcritical flow.

[‡]For the constant mode it is assumed that $\lambda \rightarrow \infty$ or $k \rightarrow 0$ so that $L_0 = \lim_{k \rightarrow 0} L = \rho g (Fr^2 - 1)$.

[§]As only a finite number of Fourier modes is taken into account for $\boldsymbol{F}_{\text{st}}$, L will usually not become exactly zero and $\boldsymbol{F}_{\text{st}}$ will only be nearly singular.

3.3 | Quasi-Newton solution method for supercritical steady free surface flow

The steady free surface problem is now stated more precisely, using the same free surface discretization as in the previous section ($\boldsymbol{\eta}, \boldsymbol{p} \in \mathbb{R}^{n \times 1}$ and uniformly distributed points). \mathcal{F} is a non-linear black-box flow solver for a general 2D steady free surface flow problem (inviscid or viscous flow, arbitrary geometry below the free surface):

given the flow solver $\mathcal{F}(\boldsymbol{\eta}) = \boldsymbol{p}$ which fulfills the KBC and tangential DBC, find $\boldsymbol{\eta}$ so that the normal DBC $\boldsymbol{p} = p_{\text{cst}} \mathbf{1}$ is fulfilled.

As mentioned above, the KBC from Eq. (4) and tangential DBC from Eq. (6) are fulfilled by modeling the free surface boundary as a free-slip wall in the flow solver. In order for the normal DBC to be meaningful, it is assumed that a fixed location is used as pressure reference.

It is assumed that \mathcal{F} is a bijective function for supercritical flow, as was motivated in the last paragraph of Section 3.2 by analyzing the surrogate model \mathcal{F}_{st} . This means that for every value of p_{cst} , the system has a unique solution $\boldsymbol{\eta}$. As only the gradient of the pressure appears in the incompressible Navier-Stokes equations (Eq.(2)), the pressure reference in the flow solver \mathcal{F} can be chosen at an arbitrary location in the domain. For a given choice, the value of p_{cst} will thus determine the depth of the flow. However, it is more straightforward to directly impose the inlet height $\boldsymbol{\eta}(0)$ to fix the depth. p_{cst} then becomes an unknown which is not of interest. It can be removed from the problem by filtering out the constant Fourier mode (i.e. the average value). With

$$\boldsymbol{p}_\emptyset = (\mathbf{I}_n - \Phi_0) \boldsymbol{p} \quad (17)$$

$$\mathcal{F}_\emptyset = (\mathbf{I}_n - \Phi_0) \mathcal{F} \quad (18)$$

the free surface problem becomes:

given the flow solver $\mathcal{F}_\emptyset(\boldsymbol{\eta}) = \boldsymbol{p}_\emptyset$ which fulfills the KBC and tangential DBC, find $\boldsymbol{\eta}$ so that the normal DBC $\boldsymbol{p}_\emptyset = \mathbf{0}$ and the inlet height condition $\boldsymbol{\eta}(0) = h$ are fulfilled.

This problem has to be solved iteratively: in each iteration m the flow field is solved by calling the black-box flow solver without constant mode \mathcal{F}_\emptyset , then the new free surface position $\boldsymbol{\eta}^{m+1} = \boldsymbol{\eta}^m + \Delta\boldsymbol{\eta}^m$ is calculated and the mesh updated accordingly. Newton's method can be used to calculate $\Delta\boldsymbol{\eta}^m$ as

$$\mathcal{F}'_\emptyset \Delta\boldsymbol{\eta}^m = -\boldsymbol{p}_\emptyset^m \quad \text{with} \quad \boldsymbol{\eta}^{m+1}(0) = h \quad (19)$$

where \mathcal{F}'_\emptyset is the Jacobian of \mathcal{F}_\emptyset . As the flow solver is considered a black-box, its Jacobian is not known and an approximation $\widehat{\mathcal{F}'_\emptyset}$ is used. Rewriting the inlet condition, a linear system emerges to calculate $\Delta\boldsymbol{\eta}^m$:

$$\begin{cases} \widehat{\mathcal{F}'_\emptyset} \Delta\boldsymbol{\eta}^m = -\boldsymbol{p}_\emptyset^m \\ \Delta\boldsymbol{\eta}^m(0) = h - \boldsymbol{\eta}^m(0) \end{cases} \quad (20)$$

The surrogate model \mathcal{F}_{st} from Eq. (16) is used in a first approximation of \mathcal{F}'_\emptyset :

$$\widehat{\mathcal{F}'_{\emptyset, \text{sur}}} = (\mathbf{I}_n - \Phi_0) \mathcal{F}'_{\text{st}} \quad (21)$$

To stabilize and accelerate the iterations, a second approximation to \mathcal{F}'_\emptyset is constructed using the IQN-ILS algorithm by Degroote et al.¹¹ This is used in fluid-structure interaction to improve convergence of coupling iterations. The idea is to use known input-output pairs of a black-box to construct an approximate Jacobian for it, which improves with each iteration. In this case, the input of the black-box \mathcal{F}_\emptyset is $\boldsymbol{\eta}$, the output \boldsymbol{p}_\emptyset . Differences between consecutive iterations are stored in the matrices

$$\mathbf{V}^m = [\Delta\boldsymbol{\eta}^{m-1} \quad \dots \quad \Delta\boldsymbol{\eta}^0], \quad (22)$$

$$\mathbf{W}^m = [\Delta\boldsymbol{p}_\emptyset^{m-1} \quad \dots \quad \Delta\boldsymbol{p}_\emptyset^0]. \quad (23)$$

These matrices are used to construct the approximate Jacobian with a least-squares technique as

$$\widehat{\mathcal{F}'_{\emptyset, \text{IQN}}}^m = \mathbf{W}^m \mathbf{R}^{m-1} \mathbf{Q}^{mT} \quad (24)$$

with

$$\mathbf{V}^m = \mathbf{Q}^m \mathbf{R}^m \quad (25)$$

the economy-size QR-decomposition of V^m .

The two approximations of the Jacobian now have to be combined. $\widehat{\mathcal{F}}'_{\emptyset, \text{sur}}^m$ is based on the surrogate model F_{st} and is constant, while $\widehat{\mathcal{F}}'_{\emptyset, \text{IQN}}^m$ is based on the IQN-ILS algorithm and changes each iteration as the matrices V^m and W^m grow. $\widehat{\mathcal{F}}'_{\emptyset, \text{IQN}}^m$ only affects the part of $\Delta\eta^m \in \text{range}(V)$, which is equal to $Q^m Q^{mT} \Delta\eta^m$. Consequently, $\widehat{\mathcal{F}}'_{\emptyset, \text{sur}}^m$ is used for the remaining part of $\Delta\eta^m$.

The linear system to calculate $\Delta\eta^m$ for supercritical flow is

$$\begin{cases} \widehat{\mathcal{F}}'_{\emptyset}^m \Delta\eta^m = -p_{\emptyset}^m \\ \Delta\eta^m(0) = h - \eta^m(0) \end{cases} \quad (26)$$

with

$$\widehat{\mathcal{F}}'_{\emptyset}^m = \widehat{\mathcal{F}}'_{\emptyset, \text{IQN}}^m Q^m Q^{mT} + \widehat{\mathcal{F}}'_{\emptyset, \text{sur}}^m (I_n - Q^m Q^{mT}) \quad (27)$$

$$= W^m R^{m-1} Q^{mT} + (I_n - \Phi_0) F_{\text{st}} (I_n - Q^m Q^{mT}). \quad (28)$$

The Jacobian approximation $\widehat{\mathcal{F}}'_{\emptyset}^m$ has rank $n - 1$, because the constant mode is not part of its column space. By adding the inlet condition $\eta(0) = h$, the system in Eq. (26) with n unknowns becomes rank n and has a unique solution. However, as it has $n + 1$ equations for n unknowns, it is solved with a least-squares method.

Algorithm 1 outlines the new free surface method. For compactness the left- and right-hand side matrices of Eq. (26) are denoted respectively by $A^m \in \mathbb{R}^{(n+1) \times n}$ and $b^m \in \mathbb{R}^{(n+1) \times 1}$, so that the system can be written in the form $A^m \Delta\eta^m = b^m$.

Algorithm 1 Free surface Quasi-Newton method with Least-Squares and Surrogate (FrQ-LeSS).

```

1:  $m = 0$ 
2:  $p_{\emptyset}^0 = \mathcal{F}_{\emptyset}(\eta^0)$   $\triangleright \mathcal{F}_{\emptyset} = (I_n - \Phi_0) \mathcal{F}$ 
3: while  $\|p_{\emptyset}^m\|_2 > \varepsilon$  do
4:   if  $m > 0$  then
5:     construct  $V^m, W^m$ 
6:     calculate QR-decomposition  $V^m = Q^m R^m$ 
7:   end if
8:   construct  $A^m$  and  $b^m$   $\triangleright \text{Fr} > 1$ : Eq. (26),  $\text{Fr} < 1$ : Eq. (30)
9:   solve  $A^m \Delta\eta^m = b^m$  with least-squares
10:   $\eta^{m+1} = \eta^m + \Delta\eta^m$ 
11:   $m = m + 1$ 
12:   $p_{\emptyset}^m = \mathcal{F}_{\emptyset}(\eta^m)$ 
13: end while

```

3.4 | Modifications for subcritical flow

As argued in Section 3.2, for subcritical flow \mathcal{F} is not a bijection anymore due to the presence of the steady gravity wave, so two additional conditions must be added to find a unique η for given p . A plausible, physically-relevant option is to insist that the free surface is unperturbed (flat) at the inlet, which can be expressed as

$$\eta(i) = h \quad i = i_1, i_2 \quad (29)$$

with i_1 and i_2 two points close to the inlet. The system for supercritical flow from Eq. (26) is adapted to

$$\begin{cases} \widehat{\mathcal{F}}'_{\emptyset}^m \Delta\eta^m = -p_{\emptyset}^m \\ \Delta\eta^m(i) = h - \eta^m(i) \quad i = 0, i_1, i_2. \end{cases} \quad (30)$$

The Jacobian is approximated in exactly the same way as before. The matrices $A \in \mathbb{R}^{(n+3) \times n}$ and $b \in \mathbb{R}^{(n+3) \times 1}$ are again introduced to write the system of Eq. (30) in the form $A^m \Delta\eta^m = b^m$. The iteration scheme is the same as for supercritical flow and given by Algorithm 1.

As the steady wave frequency will usually not coincide exactly with a discrete Fourier mode, the system from Eq. (30) can be slightly overdetermined in practice. The solution is then no longer unique and the least-squares solver returns the solution $\Delta\eta^m$ for which the residual $\mathbf{b}^m - \mathbf{A}^m\Delta\eta^m$ is minimal in the L^2 -norm. The Fourier mode with wavenumber closest to the steady wave has $L \approx 0$ and the smallest contribution to the residual. It is therefore this mode whose phase and amplitude are most significantly influenced by the added inlet conditions. To ensure that the auxiliary conditions have enough influence, the three inlet conditions in Eq. (30) must be multiplied (or *weighed*) with a factor much larger than the smallest value of $|L|$.

4 | NUMERICAL EXPERIMENTS

4.1 | General settings

In this section, the FreQ-LeSS method is tested on two 2D cases for which experimental data is available. Both have been used in several papers for testing fitting and capturing approaches. Before introducing these cases, some settings which are used in all simulations are reported. The finite volume flow solver ANSYS Fluent is used to solve the RANS equations with the SST $k-\omega$ turbulence model by Menter.¹² In all boundary layers a $y^+ < 5$ is ensured. All convection terms are discretized with a second-order upwind scheme. The properties of water at 20 °C are used: $\rho = 998.2 \text{ kg/m}^3$, $\nu = 10^{-6} \text{ m}^2/\text{s}$. Boundary conditions are similar in all simulations: a velocity profile at the inlet, a hydrostatic pressure profile at the outlet, no-slip conditions at the bottom wall and free-slip conditions at the free surface. In all simulations the initial free surface η^0 is horizontal and has height h . The pressure reference point in the flow solver is always the bottom-right point of the fluid domain.

To apply a new free surface position, the mesh must be deformed. This operation is considered to be part of the black-box flow solver and therefore of lesser relevance to this paper. However, it can be noted that the deformations encountered in steady free surface flows are generally small and should not pose any problems. This is the case because waves start to break –and consequently the flow becomes unsteady– at small ratios between waveheight and wavelength. In deep water, breaking occurs when this ratio is around 0.17, in shallow water the value is also function of the water depth.¹³ As illustration, for both test cases that will be introduced later in this section, the experiments showed wave breaking starting at a ratio around 0.10.

For completeness, the mesh update strategy used here is described briefly. The mesh is deformed during the surface updates by stretching in the vertical direction. Normally the free surface deformation would be linearly interpolated over the entire depth, becoming zero at the bottom. For flow over a hydrofoil (Section 4.5) this is not possible, as the hydrofoil itself would be deformed. The solution is to choose a minimum height y_{\min} (somewhere above the hydrofoil), below which the mesh is not deformed, and use this as reference position instead of the bottom to interpolate the free surface deformation to the interior nodes. To be consistent, the same approach is used for the flow over a bottom topography. It resulted in good mesh quality in all cases. An alternative approach could be to couple the flow solver to an elliptic mesh generator to obtain good quality, deforming structured meshes.^{14,15}

4.2 | Pressure extrapolation

Depending on the flow solver, the pressure can be stored at different locations on the mesh. The solver used for this paper uses a collocated scheme where all variables are stored at the cell centers. As the fitting method is based on the pressures at the free surface nodes, pressures at the cell centers must be extrapolated to these nodes. One possible method is to extrapolate the pressures from the downstream and upstream cells using the cell gradients, and then taking the average of the two, but this does not give a physically relevant value as will be shown.

Fig. 4 (top) shows a high frequency oscillation of the free surface (dashed line) and how it is discretized (full line) with quad elements. The cell centers C and free surface nodes N are indicated. Fig. 4 (bottom) schematically shows the corresponding pressure distribution in the x -direction, ignoring the vertical offset between the cell centers and the free surface for now. The dashed line is the value predicted by the perturbation analysis for a sinusoidal wave (Section 3.1). In the cell centers this gives a constant pressure, i.e. the oscillation is not visible when discretized. The full line is the actual CFD result. Flow is from left to right, so the pressure oscillation has shifted downstream over a quarter wavelength and is visible in the cell centers. This asymmetry is due to the upwind discretization of the momentum convection: physical oscillations in both pressure and velocity are shifted downstream with half a cell. To get the correct pressure oscillation at the free surface nodes, pressure is extrapolated from the downstream cells as indicated in Fig. 4 with red arrows. In the example (Fig. 4) the discrete pressure gradient in the

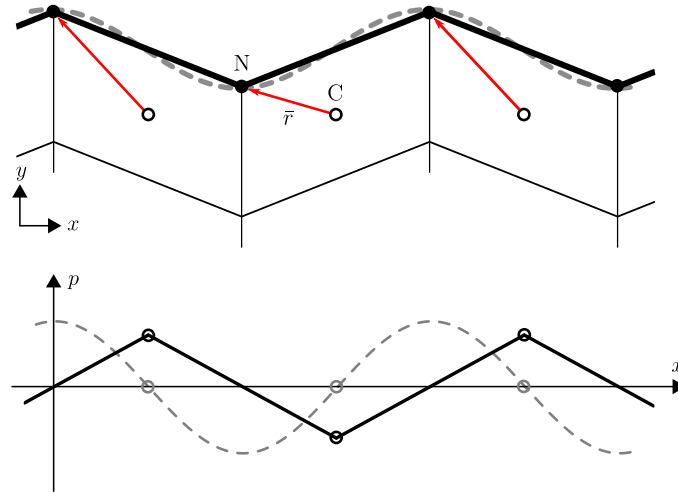


FIGURE 4 At the top, a high frequency oscillation (dashed line) of the free surface height is shown and how it is discretized (full line). At the bottom, the corresponding pressure distribution is shown (theoretical: dashed line, CFD: full line). The red arrows indicate from which cells the free surface node pressures are extrapolated (flow from left to right).

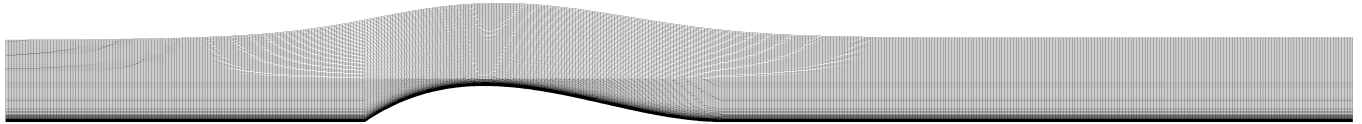


FIGURE 5 Mesh used for supercritical flow over bottom topography, with 480 free surface cells, after 20 iterations.

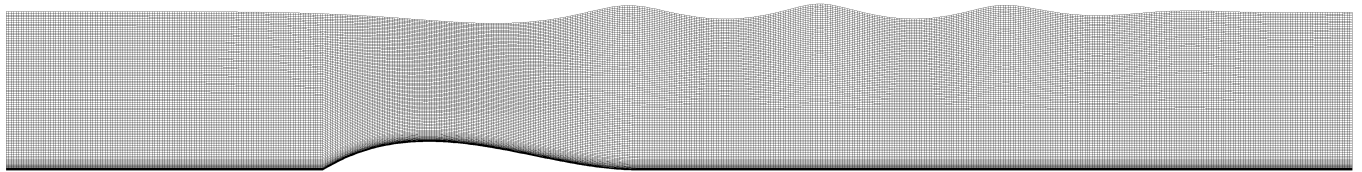


FIGURE 6 Mesh used for subcritical flow over bottom topography, with 544 free surface cells, after 30 iterations.

cell centers is zero in the x -direction, so that

$$p_N = p_C + \nabla p|_C \cdot \bar{r} = p_C + \left. \frac{\partial p}{\partial y} \right|_C (y_N - y_C). \quad (31)$$

This means the node pressure is equal to the downstream cell pressure plus a height correction.

Assuming the free surface grid is sufficiently fine, high frequency oscillations as described here are unphysical and will not be present in the final solution. It is however possible that they appear during the iterative process and become unstable. It is therefore very important that extrapolation is done in the described way, so that high frequency oscillations appear in the pressure and have the correct phase, which ensures that they are effectively damped by the surrogate model. This approach has been tested for a wide range of upwind convection schemes: first and second order upwind schemes, a power scheme, a QUICK-like scheme and a third order MUSCL scheme. It always worked and thus seems to be widely applicable.

4.3 | Supercritical flow over bottom topography

The first test case studies the flow over a bottom topography, as shown in Fig. 5. The flow direction is from left to right. The shape of the bottom obstacle is described by

$$y_b = \frac{27}{4} \frac{H_b}{L_b^3} x(x - L_b)^2 \quad \text{for } 0 \leq x \leq L_b \quad (32)$$

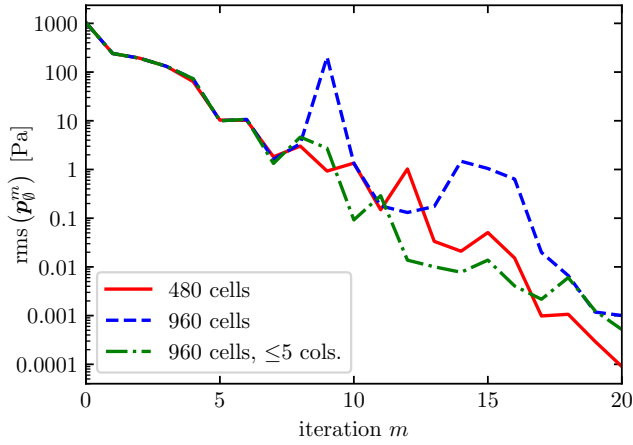


FIGURE 7 Residuals for supercritical flow over bottom topography, for meshes with 480 and 960 cells at the free surface and with all the columns or at most 5.

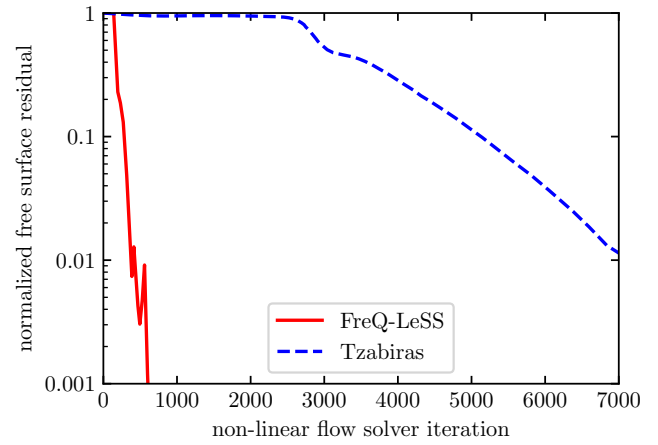


FIGURE 8 Comparison of normalized residuals as a function of flow solver iterations, for supercritical flow over bottom topography.

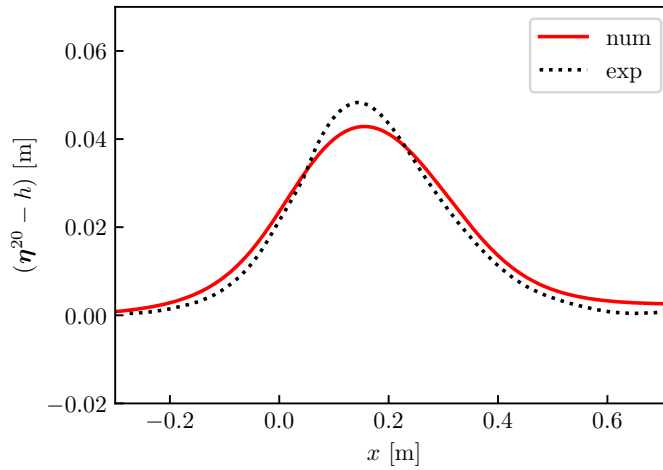


FIGURE 9 Numerical and experimental free surface for supercritical flow over bottom topography.

where $L_b = 0.42$ m is the length and $H_b = 0.042$ m the height of the obstacle. Experimental data for supercritical and subcritical flows has been acquired by Cahouet.¹⁶ This test case has been used previously for evaluating fitting methods^{6,5} and capturing methods.^{17,18} The supercritical case has an inlet velocity profile with mean value $U = 1.98$ m/s and inlet height $h = 0.0955$ m, giving a Froude number of $Fr = 2.05$. The simulation domain extends from $x = -L_b$ to $x = 2.75L_b$, minimizing the influence of the boundaries on the solution. Fig. 5 shows the structured mesh which is used. In the x -direction it is uniform (128 cells per length L_b , i.e. 480 in total), in the y -direction it resolves the bottom boundary layer. The minimum height for the mesh deformation is chosen as $y_{\min} = 1.2H_b$.

The error of the iterative method with respect to the dynamic boundary condition is the free surface pressure p_θ . The residual which characterizes convergence is defined as the root mean square of p_θ . This value is shown in Fig. 7 as a function of the free surface update iterations: its convergence behavior is clearly exponential.

In a second simulation, the number of unknowns is doubled by splitting each cell of the domain in the x -direction. Residuals for this case are also shown in Fig. 7: the mesh refinement barely has an influence on the convergence speed of the quasi-Newton method, but a high peak now appears in the pressure residual in iteration 9. A closer look reveals that this is caused by $\widehat{\mathcal{F}}_{\theta, \text{IQN}}^m$ giving a bad prediction in the previous iteration, which can be explained as follows. The approximate Jacobian $\widehat{\mathcal{F}}_{\theta, \text{IQN}}^m$ is a linear description of the behavior of the non-linear flow solver in the neighborhood of the current surface position. It is constructed with a least-squares technique using inputs and outputs of the flow solver from all prior iterations. During the first few iterations,

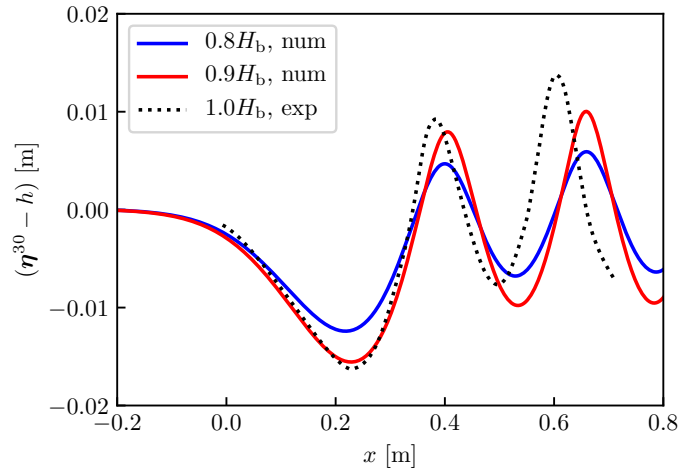


FIGURE 10 Numerical and experimental free surface for subcritical flow over bottom topography.

the free surface displacements are very big, which means they will not give a good description of the flow solver in a later iteration as the surface position is then very different. If the number of columns in \mathbf{V}^m and \mathbf{W}^m (Eqs. (22) and (23)) is limited to 5—the oldest columns are removed—the peak disappears as shown in Fig. 7. Convergence is smoother, but in the end not faster, as the IQN-ILS algorithm with all columns effectively compensates the errors it introduces in subsequent iterations.

Tzabiras⁶ used the same test-case to evaluate a time-stepping method where the DBC is fulfilled in the flow solver, and the KBC is used to update the free surface height. In that case the residual was defined such that it is proportional to the L^2 -norm of the mass flow rate through the free surface. Whereas it takes ~ 500 iterations to reduce the residual an order of magnitude with the time-stepping method, only ~ 3 are needed with the FreQ-LeSS method.

The total number of non-linear flow solver iterations (e.g. SIMPLE algorithm) are a good indication to correctly assess the speedup of the new method with respect to a time-stepping method. This is done for the coarse mesh (544 free surface cells), as it is roughly similar in size to the one used by Tzabiras. In the previous simulations, the focus was on the number of surface updates, so the flow solver was run to deep convergence in each step. The criterion was calculated by summing the absolute value of the mass creation over all cells, followed by a division by the largest value of this sum in the first five iterations. To minimize the number of flow solver iterations, a less stringent convergence criterion is chosen. It is important that the free surface pressure converges deep enough, as it is used as input for both the quasi-Newton iteration and the least-squares approximate Jacobian $\widehat{\mathbf{F}}'_{\theta, \text{IQN}}$. Therefore, a convergence criterion based on the free surface pressure is introduced:

$$\frac{\text{rms}(\mathbf{p}^j - \mathbf{p}^{j-1})}{\max(\text{rms}(\mathbf{p}^j), \epsilon)} < 10^{-3} \quad (33)$$

with j the current non-linear flow solver iteration and ϵ a small number (e.g. 10^{-16}). Fig. 8 compares the residuals as a function of the non-linear flow solver iterations between FreQ-LeSS and Tzabiras. A large speedup is visible.

The converged free surface position is compared to the experimental result in Fig. 9. Overall, there is good agreement between the computed results and the experimental data, but there is a noticeable difference in crest height. The result however falls within the uncertainty margins of the experimental data.^{6,16} References which use the same test case by Cahouet, often do this with simplifying assumptions: free-slip conditions at the bottom and inviscid or laminar flow.^{17,18,19} The result by Tzabiras⁶ does not use these simplifications. When the current results are compared with those by Tzabiras, a height difference of only $\sim 1\%$ is found.

4.4 | Subcritical flow over bottom topography

The bottom topography described in Section 4.3 was also tested by Cahouet¹⁶ for subcritical flow with parameters $\text{Fr} = 0.43$ and $h = 0.21$ m.

For subcritical flow two additional conditions (Eq. (29)) are added to the system to specify that the free surface has to be unperturbed in the inlet region. More specifically: $\eta(i_1)$ and $\eta(i_2)$ must both be equal to h , just as $\eta(0)$. The points i_1 and i_2

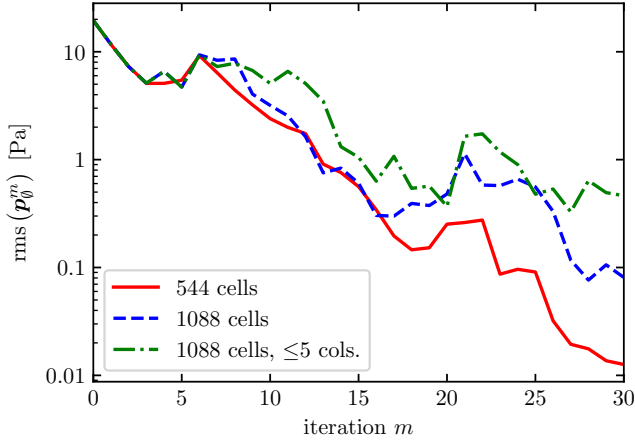


FIGURE 11 Residuals for subcritical flow over bottom topography, for meshes with 544 and 1088 cells at the free surface and with all the columns or at most 5. The numerical values were obtained with the reduced height of $0.9H_b$.

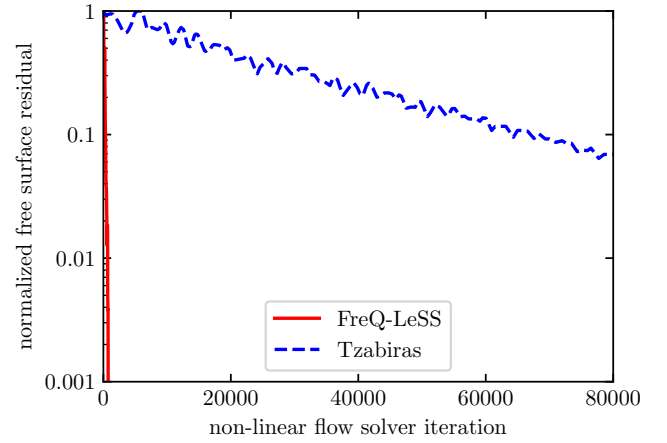


FIGURE 12 Comparison of normalized residuals as a function of flow solver iterations, for subcritical flow over bottom topography.

should be close enough to the inlet so that the inlet length of the domain can be minimized. However, they may not be too close to the inlet either: when e.g. values $i_1 = 1$, $i_2 = 2$ are used, the method becomes highly sensitive to small fluctuations in the free surface position, which can lead to very large updates $\Delta\eta$ and therefore bad convergence behavior of the iterative method. It makes more sense to choose physically meaningful positions independent of the discretization: i_1 and i_2 are chosen at distances $\lambda_{sw}/8$ and $\lambda_{sw}/4$ from the inlet, where λ_{sw} is the wavelength of the steady gravity wave. The three equations at the inlet are multiplied with a factor $\max(L) \times 10^4$, as lower values hindered deep convergence in some cases.

For supercritical flow the free surface consists of a single wave crest above the bottom topography (Fig. 5). For subcritical flow a trailing wave pattern develops behind the flow disturbance (Fig. 6). This wave train reflects at the hydrostatic outlet, rendering the solution meaningless. To avoid reflections at the downstream boundary, the surface waves are artificially damped towards the outflow boundary by introducing dissipation terms in the momentum equations. Following the description by Peric et al.²⁰, these terms take the form

$$\int_V \rho q_i dV \quad (34)$$

where

$$q_i = \gamma b(x)(u_{i,\text{ref}} - u_i), \quad i = x, y. \quad (35)$$

These terms force the flow solution to given reference velocities $u_{x,\text{ref}}$ and $u_{y,\text{ref}}$, which are based on the mass flow rate and free surface slope at the outlet. If the free surface is not horizontal due to flow losses, it is important that $u_{y,\text{ref}} \neq 0$, otherwise some reflection occurs. The term $b(x)$ is a blending function, which gradually activates the damping in a region of length l_d at the outlet. A \cos^2 function is used for the blending, described by

$$b(x) = \begin{cases} \cos^2\left(\frac{\pi}{2l_d}(x - x_{\text{out}})\right), & x \geq x_{\text{out}} - l_d \\ 0, & x < x_{\text{out}} - l_d \end{cases} \quad (36)$$

with $x_{\text{out}} = \mathbf{x}(n-1)$ the outlet's x-position. The length l_d is chosen as $1.5L$, which is roughly $2.5\lambda_{sw}$. The wavelength of the (non-linear) trailing wave which has to be damped out, is close to the linear prediction λ_{sw} . The longer the damping zone, the more gradual the damping can be done and the better the results: 2.5 times the wavelength should give very good damping according to the theory. Peric et al.²⁰ present a method to estimate the optimal forcing strength γ for given wave and damping parameters. Based on this the value $\gamma = 15$ was chosen.

The auxiliary flat-surface conditions at the inlet effectively suppress upstream waves, and cause a steady gravity wave to appear only in the domain behind the obstacle. Especially in the first few iterations large deformations may occur. It was observed that this gives overshoot of the free surface solution, so by using some underrelaxation on $\Delta\eta^m$ the iterations converge faster. As the mesh deformations are smaller due to the relaxation, the flow solver also converges faster in each iteration. Outside the damping zone a relaxation factor of 0.5 is used, which is reduced to a factor 0.2 at the outlet, using again the blending function from

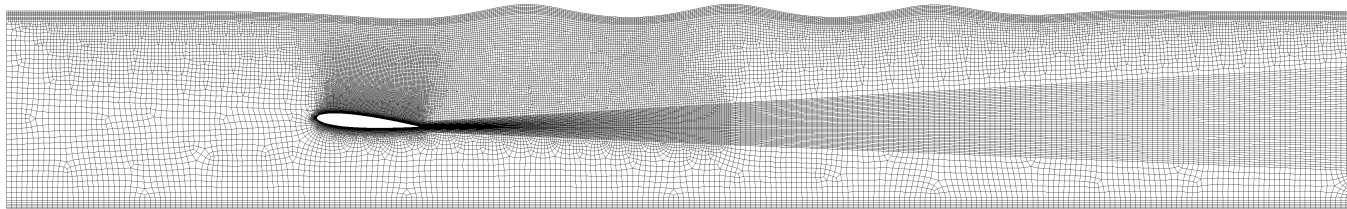


FIGURE 13 Mesh used for subcritical flow over hydrofoil, with 650 free surface cells, after 15 iterations.

Eq. (36). This is done to decrease wave formation in the damping zone, as those waves need to be damped out anyway. After 20 iterations the relaxation is turned off, as $\Delta\eta^m$ is now very small and relaxation is not useful anymore.

The calculation mesh shown in Fig. 6 is very similar to the one for supercritical flow. The domain extends from $x = -L_b$ to $x = 3.25L_b$ and the number of cells is again 128 per L_b , giving a total of 544 cells at the free surface. The minimum height for the mesh deformation is chosen as $y_{\min} = 2H_b$.

The parameters as reported by Cahouet ($Fr = 0.43$, $h = 0.21$ m) give rise to steep non-linear waves which are close to breaking (see Fig. 10). Simulations with the parameters from the experiments give even higher waves which are unstable so that no steady solution can be found. A likely reason seems to be that the flow is somewhat unstable at these conditions and the free surface has no real steady state. This is supported by two observations. Firstly, the raw data measured by Cahouet shows height fluctuations of ~ 5 mm, which is certainly not negligible when looking at the wave amplitude in Fig. 10. Secondly, the time-stepping method of Tzabiras⁶ did not converge to a steady solution for this case, while it did converge for the cases in Sections 4.3 and 4.5. Instead oscillating behavior was found and the relative free surface residual did not go much below 10%. Furthermore, the numerical solution (wavelength, amplitude) was found to be very sensitive to variations of the inlet turbulence and velocity profile, which are both not clearly reported by Cahouet.

To obtain a steady state solution in the simulation, it was run for bottom topographies with reduced heights $0.9H_b$ and $0.8H_b$ in Eq. (32), keeping all other parameters constant. As can be seen in Fig. 10 the resulting waves increase quickly in amplitude with increasing height of the obstacle, and the wavelength grows shorter in accordance with non-linear wave theory.⁹

Convergence of the fitting method is shown in Fig. 11 for the original mesh and a refined one. The plotted residual is calculated on the domain without the damping zone, i.e. from $x = -L_b$ to $1.75L_b$. Convergence is somewhat slower than for supercritical flow, but still decreases exponentially and essentially independent of the mesh size. For the fine mesh, results are also shown with a limited number of columns for \mathbf{V}^m and \mathbf{W}^m . For this subcritical case, reducing the number of columns opposes convergence; clearly IQN-ILS needs a larger number of modes compared to supercritical flow. Convergence can again be compared to other fitting methods: the time-stepping method by Tzabiras⁶ and the steady iterative method by van Brummelen et al.⁵ which was mentioned in Section 1. The latter also updates the free surface based on the normal DBC, so the definition of the residual is very similar to this paper. The time-stepping method needs $\sim 10^4$ iterations to reduce the residual by a factor ten, the steady iterative method ~ 4 and the FreQ-LeSS method ~ 10 . The steady iterative method needs fewer iterations thanks to the combined free surface condition which gives stronger coupling. The new method compensates for this by being compatible with black-box flow solvers. Analogous to the supercritical flow, convergence speed is compared between FreQ-LeSS and a time-stepping method in Fig. 12. For the former the convergence criterion from Eq. 33 is used, for the latter the best result from Tzabiras is taken.

4.5 | Subcritical flow over hydrofoil

The second case which is considered is that of the flow over a hydrofoil. In the original paper by Duncan²¹ experiments were done to study the resistance on a hydrofoil caused by breaking and non-breaking waves. A NACA0012 profile with chord $c = 0.203$ m was pulled through stagnant water at an angle of attack of 5° , a velocity of 0.8 m/s, at 0.175 m above the bottom and at a given submergence beneath the undisturbed free surface level. At large submergences, a non-breaking trailing wave pattern developed, at small submergences a breaking wave pattern. Transition between these two regimes took place at a submergence of 0.193 m. The non-breaking cases have been used for validating both fitting^{6,22} and capturing²³ methods. The non-breaking case which is simulated here has a submergence of 0.21 m, so that $h = 0.385$ m and $Fr = 0.412$.

The same settings are used for some of the parameters which were introduced in Section 4.4 to simulate subcritical flow: for the points i_1 and i_2 , for the damping length ($l_d = 5c \approx 2.5\lambda_{sw}$) and for the relaxation of $\Delta\eta^m$. As this case converges faster, relaxation is turned off after 10 iterations. The damping factor is chosen in the same way, giving $\gamma = 12$.

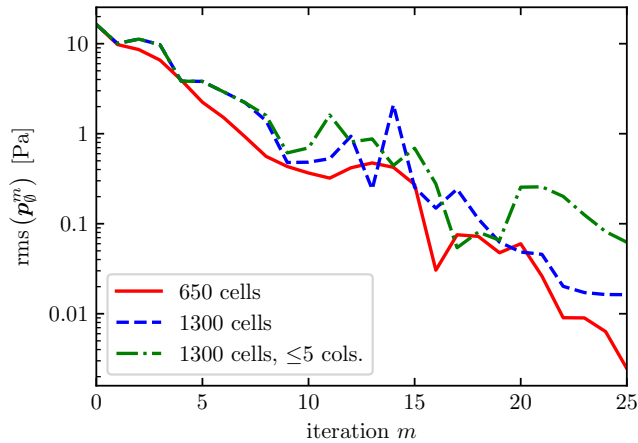


FIGURE 14 Residuals for subcritical flow over hydrofoil, for meshes with 650 and 1300 cells at the free surface and with all the columns or at most 5.

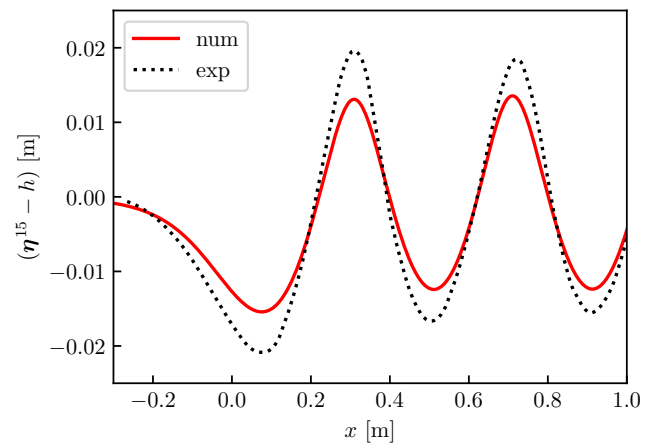


FIGURE 15 Numerical and experimental free surface for subcritical flow over hydrofoil.

The domain stretches from $x = -3c$ to $x = 10c$, with the hydrofoil's leading edge located at $x = 0$ m. The mesh used in the simulations is shown in Fig. 13. At the bottom and the free surface a layer of structured mesh is used, around the hydrofoil and in the wake a C-mesh, and in the rest of the domain an unstructured quad-dominant mesh. This strategy reduces the cell count compared to a fully structured mesh, while having good discretization of the hydrofoil (325 cells on hydrofoil wall). The free surface is meshed uniformly with 650 cells. The minimum height for the mesh deformation is chosen as $y_{\min} = 0.175 + c/2$.

In Fig. 14 convergence of the residuals is shown for the original mesh and a refined one. The damping zone is again not taken into account. Convergence is very similar to the subcritical flow over a bottom topography, i.e. the residuals decrease exponentially. Reducing the number of columns in the IQN-ILS approximation again gives worse convergence.

Fig. 15 compares the experimental free surface with the computed one. The wavelength corresponds well, the amplitude is underestimated. The reason is that the hydrofoil boundary layer cannot be modeled correctly in a steady state setting. The Reynolds number for the hydrofoil is low (1.62×10^5), the inlet turbulence is not known, but it should also be low as the hydrofoil is pulled through stagnant water. As a consequence there is a large laminar region on both sides of the hydrofoil. The transition from laminar to turbulent flow can be predicted using the local correlation-based transition model by Menter et al.²⁴, but due to instabilities in the suction side transition the flow becomes unsteady. Therefore, transition modeling was not taken into account for the final results; the fully turbulent SST $k-\omega$ model was used instead.

5 | CONCLUSIONS

In this paper the *Free surface Quasi-Newton method with Least-Squares and Surrogate* (FreQ-LeSS) is presented. It solves the free-boundary problem of 2D steady free surface flow where the free surface is represented by fitting. The new method combines two attractive properties. Firstly, the method can work with a black-box flow solver, as the KBC and tangential DBC at the free surface are easily enforced using a free-slip wall. Secondly, the normal DBC is used to calculate the free surface position instead of a time-stepping mechanism based on the KBC, resulting in a fast iterative method. The iterative solution algorithm is based on a quasi-Newton scheme where the Jacobian of the flow solver is approximated in two ways: by making a surrogate model based on a potential flow perturbation analysis, and by combining flow solver inputs and outputs from previous quasi-Newton iterations with a least-squares technique (IQN-ILS). To the best of the authors' knowledge, it is the first time that a quasi-Newton technique combines an approximate Jacobian from a surrogate model, with an approximate Jacobian from data collected during the iterations. For subcritical flows, a flat free surface is imposed at the inlet to get a unique solution.

The new method was tested on supercritical and subcritical flows over a bottom topography, and subcritical flow over a hydrofoil. It converges exponentially in a low number of iterations for all cases, although supercritical flow is faster. The numerical results convey that the convergence behavior of the new method is essentially independent of the free surface mesh size.

In future work, the new method will be extended to 3D steady free surface flows. The algorithm does not need to be changed, but an improved surrogate model will be needed. This model will be based on a similar perturbation analysis in 3D, and can be constructed e.g. using the convolution theorem.

References

1. Wackers J, Koren B, Raven H, et al. Free-surface viscous flow solution methods for ship hydrodynamics. *Archives of Computational Methods in Engineering* 2011; 18(1): 1–41. doi: 10.1007/s11831-011-9059-4
2. Harlow FH, Welch JE. Numerical calculation of time-dependent viscous incompressible flow of fluid with free surface. *The Physics of Fluids* 1965; 8(12): 2182–2189. doi: 10.1063/1.1761178
3. Hirt CW, Nichols BD. Volume of fluid (VOF) method for the dynamics of free boundaries. *Journal of Computational Physics* 1981; 39(1): 201–225. doi: 10.1016/0021-9991(81)90145-5
4. Sussman M, Smereka P, Osher S. A level set approach for computing solutions to incompressible two-phase flow. *Journal of Computational Physics* 1994; 114(1): 146–159. doi: 10.1006/jcph.1994.1155
5. van Brummelen EH, Raven HC, Koren B. Efficient numerical solution of steady free-surface Navier–Stokes flow. *Journal of Computational Physics* 2001; 174(1): 120–137. doi: 10.1006/jcph.2001.6880
6. Tzabiras G. A numerical investigation of 2D, steady free surface flows. *International Journal for Numerical Methods in Fluids* 1997; 25(5): 567–598. doi: 10.1002/(sici)1097-0363(19970915)25:5<567::aid-fld577>3.0.co;2-q
7. Muzafferija S, Perić M. Computation of free-surface flows using the finite-volume method and moving grids. *Numerical Heat Transfer* 1997; 32(4): 369–384. doi: 10.1080/10407799708915014
8. Demeester T, Degroote J, Vierendeels J. Stability analysis of a partitioned iterative method for steady free surface flow. *Journal of Computational Physics* 2018; 354: 387–392. doi: 10.1016/j.jcp.2017.10.053
9. Johnson RS. *A modern introduction to the mathematical theory of water waves*. 19 of *Cambridge Texts in Applied Mathematics*. Cambridge University Press . 1997
10. Demeester T, van Brummelen EH, Degroote J. Extension of a fast method for 2D steady free surface flow to stretched surface grids. In: ; 2019.
11. Degroote J, Bathe KJ, Vierendeels J. Performance of a new partitioned procedure versus a monolithic procedure in fluid–structure interaction. *Computers & Structures* 2009; 87(11): 793–801. doi: 10.1016/j.compstruc.2008.11.013
12. Menter FR. Two-equation eddy-viscosity turbulence models for engineering applications. *AIAA Journal* 1994; 32(8): 1598–1605. doi: 10.2514/3.12149
13. Dean RG, Dalrymple RA. *Coastal processes with engineering applications*. Cambridge University Press . 2004
14. Chatzidai N, Giannousakis A, Dimakopoulos Y, Tsamopoulos J. On the elliptic mesh generation in domains containing multiple inclusions and undergoing large deformations. *Journal of Computational Physics* 2009; 228(6): 1980–2011. doi: 10.1016/j.jcp.2008.11.020
15. Fraggedakis D, Papaioannou J, Dimakopoulos Y, Tsamopoulos J. Discretization of three-dimensional free surface flows and moving boundary problems via elliptic grid methods based on variational principles. *Journal of Computational Physics* 2017; 344: 127–150. doi: 10.1016/j.jcp.2017.04.060
16. Cahouet J. *Etude numérique et expérimentale du problème bidimensionnel de la résistance de vagues non-linéaire*. Ecole Nationale Supérieure de Techniques Avancées . 1984.
17. Wackers J, Koren B. A surface capturing method for the efficient computation of steady water waves. *Journal of Computational and Applied Mathematics* 2008; 215(2): 618–625. doi: 10.1016/j.cam.2006.03.056

18. Huang J, Carrica PM, Stern F. Coupled ghost fluid/two-phase level set method for curvilinear body-fitted grids. *International Journal for Numerical Methods in Fluids* 2007; 55(9): 867–897. doi: 10.1002/fld.1499
19. van Brummelen EH, Segal A. Adjoint shape optimization for steady free-surface flows. *International Journal for Numerical Methods in Fluids* 2002; 40(3-4): 605–614. doi: 10.1002/fld.305
20. Perić R, Abdel-Maksoud M. Analytical prediction of reflection coefficients for wave absorbing layers in flow simulations of regular free-surface waves. *Ocean Engineering* 2018; 147: 132–147. doi: 10.1016/j.oceaneng.2017.10.009
21. Duncan JH. The breaking and non-breaking wave resistance of a two-dimensional hydrofoil. *Journal of Fluid Mechanics* 1983; 126: 507–520. doi: 10.1017/s0022112083000294
22. Hino T. An Unstructured Grid Method for Incompressible Viscous Flows with a Free Surface. *AIAA Paper 97-0862* 1997. doi: 10.2514/6.1997-862
23. Di Mascio A, Broglia R, Muscari R. On the application of the single-phase level set method to naval hydrodynamic flows. *Computers & Fluids* 2007; 36(5): 868–886. doi: 10.1016/j.compfluid.2006.08.001
24. Menter FR, Smirnov PE, Liu T, Avancha R. A one-equation local correlation-based transition model. *Flow, Turbulence and Combustion* 2015; 95(4): 583–619. doi: 10.1007/s10494-015-9622-4

